Defect-Free Single-Crystal SiGe: A New Material from Nanomembrane Strain Engineering

Deborah M. Paskiewicz,† Boy Tanto,† Donald E. Savage, and Max G. Lagally*

University of Wisconsin, Madison, Wisconsin 53706, United States †These authors contributed equally to this work.

ABSTRACT Many important materials cannot be grown as single crystals in bulk form because strain destroys long-range crystallinity. Among them, alloys of group IV semiconductors, specifically SiGe alloys, have significant technological value. Using nanomembrane strain engineering methods, we demonstrate the fabrication of fully elastically relaxed $Si_{1-x}Ge_x$ nanomembranes (NMs) for use as growth substrates for new materials. To do so, we grow defect-free, uniformly and elastically strained SiGe layers on Si substrates and release the SiGe layers to allow them to relax this strain completely as free-standing NMs. These SiGe NMs are transferred to new hosts and bonded there. We confirm the high structural quality of these new materials and demonstrate their use as substrates for technologically relevant epitaxial films by growing strained-Si layers and thick, lattice-matched SiGe alloy layers on them.

KEYWORDS: SiGe substrate · strained Si · epitaxy · heterostructures

Silicon–germanium alloys play an important role in group IV electronics and photonics. Many of the materials properties of SiGe alloys can be continuously tuned with composition between that of pure Si and pure Ge. Most notably, the lattice constant of SiGe varies almost linearly with Ge composition.[1] The ability to tune the lattice constant of SiGe by varying composition has led to extensive efforts in the strain engineering of Si,[2] Ge,[3] and SiGe[4] in order to enhance electronic transport properties like charge carrier mobility,[5,6] induce new effects not seen in the bulk forms of Si or Ge, such as the electro-optic effect in strained Si,[7] and create charge confinement in heterostructures.[8] Strained-Si/relaxed SiGe heterostructures are essential in group IV quantum electronics, a current high-impact research area that requires the fabrication of two-dimensional electron gas structures (2DEGs) that can be patterned and gated to confine individual electrons into quantum qubits with long coherence times.[9,10] Furthermore, crystalline SiGe enables the integration of III–V materials into Si-based systems[11,12] and the fabrication of strain-balanced superlattice heterostructures in lattice-mismatched materials.[13,14] In many of these situations, SiGe in the form of a substrate for growth of other materials is required.

The challenge in the effective use of SiGe as a high-performance material in this manner is making it. Prior efforts, extensive in nature, have failed to meet that challenge, as detailed below. In this paper, we demonstrate the fabrication, using nanomembrane strain engineering technology, of extremely high-quality SiGe crystals that are not possible to make by earlier methods: fully elastically relaxed, single-crystalline, thin alloy sheets that can be transferred to any new handling substrate and used as a template for further epitaxial growth of more SiGe or of other materials.

Because of the large difference in melting temperatures of Si and Ge, bulk crystalline forms of SiGe do not exist for a large part of the composition range;[15] segregation, lack of compositional uniformity, and grain boundary formation are limitations in the growth of single-crystalline bulk SiGe. To reach the entire composition range, epitaxial growth of SiGe is required, but such growth also suffers from significant structural-defect problems. Two methods have been developed for creating relaxed-SiGe substrates *via* epitaxial growth. The first is growth of step-graded (*i.e.*, multiple layers with increasing Ge concentration) buffer layers of SiGe. Such materials suffer from dislocation pile-ups, creating a very rough surface, called crosshatch, and local variations in the strain relaxation of the SiGe alloy, as well as many threading dislocations in the final layer.[2]

The second approach, referred to as Ge condensation,[16,17] involves growth of a low-Ge-concentration SiGe alloy layer on SOI followed by thermal oxidation. During oxidation of the SiGe alloy, the Si preferentially oxidizes, driving the Ge farther into the film to create a higher-concentration, thinner alloy layer. The high temperatures in the

* Address correspondence to lagally@engr.wisc.edu.

Received for review April 27, 2011 and accepted June 8, 2011.

Published online June 08, 2011
10.1021/nn201547k

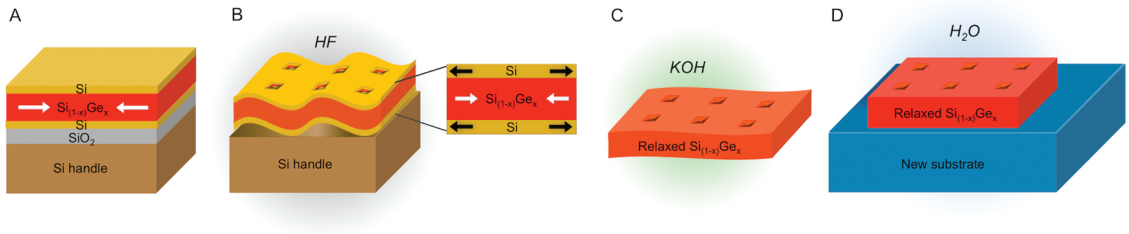

Figure 1. SiNM fabrication process. (A) SiGe and top Si layers are epitaxially grown on SOI. (B) Etchant access holes are patterned with photolithography and reactive-ion etching (RIE), then the BOX layer of the SOI is selectively etched in HF. (C) Top and bottom Si layers are selectively etched in KOH. (D) SiGe NM is transferred to a new host substrate in water and annealed to 500 °C to encourage bonding.

oxidation step encourage strain relaxation of the alloy *via* misfit dislocations, as well (*i.e.*, also plastic relaxation, as in the first method).

Both approaches therefore result in SiGe films with strain inhomogeneities, mosaic structure, and crystalline defects, ultimately limiting device performance by scattering and trapping charge carriers,[18] encouraging dopant diffusion along threading dislocations, and driving recombination of holes and electrons.[19] These performance-limiting defects become increasingly important in quantum structures, such as single-electron devices made by gating 2DEG structures.[9,10,20]

An ability to synthesize defect-free, *elastically* (rather than plastically) relaxed, single-crystalline SiGe would circumvent all of the limitations of the above methods. One would then have a new substrate for growth of thick defect-free SiGe crystals and also for the growth of strained Si and other materials without the burden of substrate defects to reduce the quality of the grown material.

As indicated above, in this paper, we demonstrate the fabrication of just such SiGe crystals. The process is as follows, shown schematically in Figure 1: We epitaxially grow a SiGe alloy layer on silicon-on-insulator (SOI) *below* the kinetic critical thickness for dislocation formation,[21] followed by a Si capping layer; this procedure creates a Si/SiGe/Si heterostructure, with the SiGe layer under compressive strain[22] (Figure 1A). To obtain high Ge concentrations in the SiGe layer, we use a concept learned from the Stranski–Krastanov growth of strained-Ge quantum dots on Si,[23] but never applied in the current context. That procedure is more fully described below. The buried oxide (BOX) layer is selectively etched away to release the Si/SiGe/Si trilayer from the SOI handling substrate (Figure 1B). In this step, the compressively strained SiGe layer shares its strain with the sandwiching Si layers. These Si layers are then selectively etched away, allowing the SiGe to elastically relax completely (Figure 1C), leaving a perfectly crystalline SiGe NM with a lattice constant appropriate to bulk SiGe at the appropriate composition.[24] We characterize the SiGe NMs throughout the fabrication process to show that the SiGe *elastically* relaxes to the bulk lattice constant during the fabrication process. Upon transfer and proper bonding to a new handle substrate, typically oxidized Si (Figure 1D; see Materials and Methods), we use the NMs for subsequent growth of thick lattice matched SiGe, as well as thin strained Si, to show that these SiGe NMs are suitable for use as a new growth substrate. We discuss how these defect-free substrates will find application in Si quantum electronics, through a potentially significant reduction in the disorder potential, variations in the electrostatic field due to defects, dislocations, and strain inhomogeneities. Controlling substrate defects and inhomogeneities may prove crucial to extend coherence lifetimes in Si spin qubits.[9,10,20,25] We point out that our nanomembrane strain engineering technique can be generalized to make many new single-crystalline materials that do not now exist.

We provide two examples of SiGe NM fabrication: (1) a ~50 nm $Si_{0.68}Ge_{0.32}$ NM that exhibits strain-driven roughening during growth, and (2) a ~50 nm $Si_{0.73}Ge_{0.27}$ NM that remains smooth during growth. The strain in the SiGe NMs is characterized throughout the fabrication process with high-resolution X-ray diffraction (XRD) and Raman spectroscopy. We monitor the surface morphology with atomic force microscopy (AFM). To demonstrate the feasibility of these transferred SiGe NMs as growth substrates, we grew 35 nm of strained Si on sample 1 with MBE and ~2 μm of lattice matched SiGe alloy plus 10 nm of strained Si on sample 2 with chemical vapor deposition (CVD). We demonstrate the quality of the resulting grown crystalline films.

RESULTS AND DISCUSSION

The as-grown Si/SiGe/Si(001) trilayer heterostructures are characterized with $\theta/2\theta$ XRD line scans through the (004) reflection. These scans (shown in Figure 2A) are fit to simulations to extract the Ge concentration and thickness of the alloy layer. The (004) reflection is a measurement of the out-of-plane lattice parameter; therefore, we expect the SiGe peak to be at a lower Bragg angle (larger plane spacing) than the Si peak. The SiGe will be compressively strained to the Si lattice parameter in-plane and, as a consequence of the Poisson effect, will expand in the out-of-plane direction. The Ge composition extracted from these

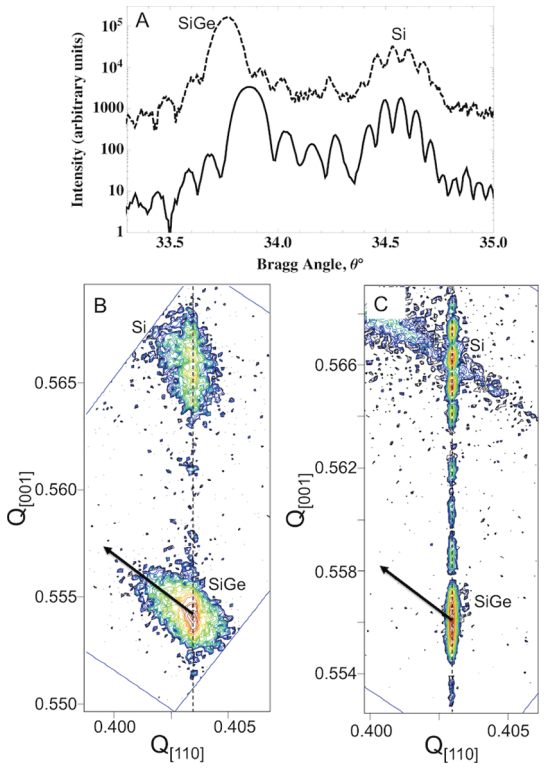

Figure 2. X-ray diffraction measurements of as-grown Si/SiGe/Si heterostructures. (A) (004) $\theta/2\theta$ line scan for 26 nm Si/55 nm $Si_{0.68}Ge_{0.32}$/27 nm Si (sample 1) [– – –] and 23 nm Si/45 nm $Si_{0.73}Ge_{0.27}$/28 nm Si (sample 2) [—]. (B) (224) off-axis reciprocal-space map (RSM) of sample 1 (rough 50 nm $Si_{0.68}Ge_{0.32}$ NM) and (C) sample 2 (smooth ~50 nm $Si_{0.73}Ge_{0.27}$ NM). The dotted vertical lines in (B) and (C) are guides for the eye to show that the Si and SiGe layers have the same in-plane lattice constant. The arrows indicate the direction along which the SiGe peak would move for a partially relaxed SiGe film. The large background signal (large diagonal streak) near the Si peak in (C) is from the underlying Si substrate. The broad (along the vertical) Si peak in (C) is modulated by thickness fringes from scattering by the alloy layer.

scans assumes that the alloy layer is fully strained to the Si lattice constant in-plane. To verify that there is no plastic relaxation in the as-grown films, off-axis reciprocal-space maps (RSMs) are taken around the (224) reflection for the two different trilayer heterostructures, as shown in Figure 2B,C. Both show that the SiGe is fully strained to the Si lattice constant; the in-plane lattice parameter is the same as that of Si. If the alloy layer were starting to relax, the SiGe peak would not have the same in-plane lattice parameter as the Si layers (horizontal peak position); the SiGe peak would start to spread and move along the relaxation arrow drawn in Figure 2B,C. The peak broadening along the relaxation line for sample 1 (Figure 2B) can be explained by the onset of strain-driven roughening that elastically relaxes the surface of the film.[26–28] This effect is more fully described below. The measurements demonstrate that the SiGe NMs remain fully strained to the Si lattice constant in the as-grown state.

At high Ge concentrations ($x > 30\%$), the alloy film may exhibit strain-driven roughening during pseudomorphic growth,[29,30] of which the classic "hut" formation of Ge on Si(001) is a prime example.[23,31] The formation of such roughness is a way for a growing film to relieve strain that competes with dislocation formation. The strain energy tends to be released plastically by dislocations when the strain is relatively small, that is, for a low-Ge-concentration SiGe alloy on Si(001). For films with larger misfit strain, for example, pure Ge on Si(001), the system prefers coherent (*i.e.*, lattice-matched) formation of individual, spatially separated 3D nanocrystals (after the 2D film "wetting layer" thickness is exceeded)[29] with a delayed onset of dislocation formation. The nucleation barrier for formation of a 3D coherently strained nanocrystal decreases rapidly with increasing strain ε as ε^{-4}, while that for formation of dislocations decreases linearly with increasing strain (*i.e.*, as ε^{-1}).[30] Hence for large strain (high Ge concentration), 3D nanocrystal formation is the preferred path to strain energy reduction. The coherent 3D nanocrystal formation allows a thicker undislocated film to be deposited for a given Ge concentration than would be possible if this mode of elastic relaxation did not exist.

This 3D nanocrystal formation elastically relaxes film strain by creating more surface area for the lattice constant to increase "outward", as shown schematically in Figure 3A for a SiGe film grown on a Si substrate. As a result, the 3D nanocrystal size that is achievable before the onset of plastic relaxation is dependent on the mismatch strain; as mismatch strain increases (Ge concentration increases) the 3D nanocrystal size decreases. Because the outward expansion occurs at the growth front of the film, the strain varies through the thickness of the SiGe layer, with the strain at the interface between the layer and substrate (point 1 in Figure 3A) equal to the mismatch strain, $\varepsilon_m = (a_{sub} - a_{film})/a_{film}$, and the average strain at the surface of the film less than the mismatch strain. The strain on the surface of the SiGe varies with the lowest strain at the peak of the nanocrystals (point 2a in Figure 3A) and highest strain at the valley of the nanocrystals (point 2b in Figure 3A). However, once this SiGe layer is released and allowed to relax elastically, there is no strain gradient through the thickness as the entire film is now elastically relaxed (lattice constant in the SiGe NM is the same at points 3 and 4 in Figure 3A), but the coherent-nanocrystal-induced surface roughness remains.

The onset of strain-driven nanocrystal formation can be controlled with growth rate and substrate temperature.[29,32] We use molecular beam epitaxy (MBE) so that we can control the growth rate and growth temperature independently, to obtain highly metastable alloy films that remain strained to the substrate lattice constant at thicknesses above the thermodynamic critical thickness.[21] Figure 3 shows results, including schematic illustrations. For 50 nm NM thicknesses, we begin to see strain-driven roughening (nanocrystal formation) at Ge concentrations of

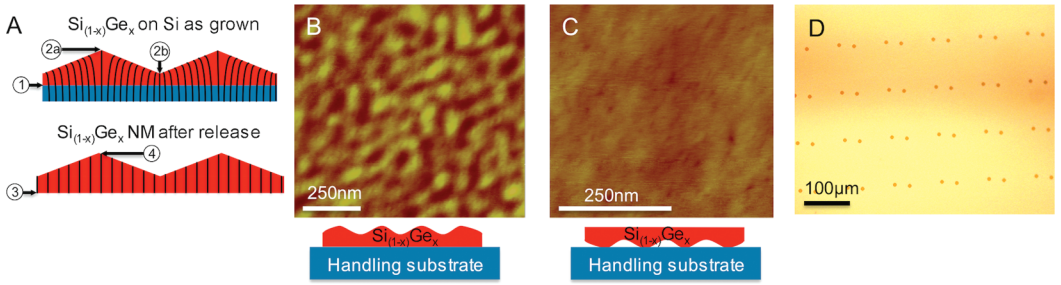

Figure 3. Three-dimensional nanocrystal formation in a ~50 nm $Si_{0.68}Ge_{0.32}$ NM. (A) Schematic diagrams illustrating the elastic relaxation of the SiGe lattice constant during formation of coherent 3D nanocrystals (top) and after release and transfer of the SiGe NM (bottom). At point 1, the SiGe is coherently strained to match the lattice constant of the underlying Si substrate. The lattice of the SiGe gradually elastically relaxes toward the top of the nanocrystal (point 2a) and becomes slightly more compressively strained at the bottom of the nanocrystal (point 2b). After release of the SiGe NM, the lattice constant in the SiGe is the same through the thickness (lattice constant at points 3 and 4 is identical in the SiGe layer). (B) AFM image of the top surface of the SiGe NM showing the onset of roughening (nanocrystal formation) due to strain minimization during growth. (C) AFM image of a similar SiGe NM that has been flipped during the release and transfer process to expose the smooth side of the SiGe NM. The schematic diagrams below the AFM images show a cross section of the sample configuration; the vertical height of the roughness is greatly exaggerated—the contact area is actually much greater than shown. (D) Optical micrograph showing an example of an asymmetric etchant access hole pattern to aid in identifying top and bottom sides of the SiGe NM.

~30% even with low growth temperatures (450–500 °C). Figure 3A illustrates that process schematically. Lower NM thicknesses allow a higher Ge concentration but are more difficult to handle in NM form. When we grow at high enough Ge concentrations and thicknesses so that coherent-nanocrystal-induced roughness forms, the released free-standing SiGe NM is flipped over upon transfer to the new handling substrate, so that the smooth side (initially the SiGe/SOI interface) of the SiGe NM is exposed for any subsequent growth (see Materials and Methods section for details). Figure 3B,C shows AFM images of a dislocation-free ~50 nm $Si_{0.68}Ge_{0.32}$ NM containing 3D nanocrystals after it has been elastically relaxed and transferred to a new host substrate (oxidized Si). Figure 3B shows the top side of the SiGe NM, and Figure 3C shows the bottom side (flipped SiGe NM). The differences in the surface morphology and root-mean-square (rms) roughness between the top and bottom surfaces are significant. The schematic diagrams below the AFM images in Figure 3B,C illustrate the sample configuration. By flipping the SiGe NM, we are able to expose the smooth side of the SiGe NM to use for subsequent growths while maintaining proper bonding to the host substrate.[24] The results here indicate that strain-driven coherent nanostructure formation does not prohibit fabrication of elastically relaxed SiGe NMs but allows much higher Ge concentrations.

We use Raman spectroscopy to monitor the strain state of the SiGe NMs throughout the fabrication process. We characterize the strain in the SiGe NMs before and after release and transfer. With knowledge of the Ge composition in the SiGe NM from XRD measurements in the as-grown state, we can measure the strain change in the SiGe NM by measuring the frequency shift of the Si–Si peak in SiGe going from the as-grown state to the released state. For biaxial strain in the (001) plane, the frequency shift is linearly proportional to strain: $\Delta\omega_{Si-Si} = b_{Si-Si}\varepsilon_{SiGe}$,[33,34] where ε_{SiGe} is the biaxial in-plane strain in the SiGe layer and b_{Si-Si} is a constant based on elastic constants and phonon deformation potentials of SiGe. The linear coefficient (b_{Si-Si}) that relates frequency shift ($\Delta\omega_{Si-Si}$) and biaxial strain (ε_{SiGe}) in SiGe has been experimentally determined to be $b_{Si-Si} = -730 \pm 70\ cm^{-1}$,[34] and it does not significantly depend on Ge concentration. Spectra from both samples are shown in Figure 4A,B. After release and transfer of the SiGe NMs, the Si–Si peaks move to lower wavenumbers, implying an increase in the in-plane lattice parameter with respect to the initial as-grown compressively strained state. Frequency shifts of -9.1 ± 0.2 and $-8.1 \pm 0.3\ cm^{-1}$ were measured for the 32 and 27% Ge composition SiGe NMs, respectively. The frequency shifts of the Si–Si modes in each of the SiGe NMs are consistent with full elastic relaxation of compressive strain from fully strained $Si_{1-x}Ge_x$ films grown pseudomorphically on Si with appropriate Ge compositions (Figure 5). The absence of a strained-Si peak in Figure 4A,B (this peak would appear between the peaks from the bulk Si and Si–Si mode of the SiGe) indicates that all of the Si was removed from the Si/SiGe/Si heterostructure during the fabrication of the SiGe NM.

After confirming full elastic relaxation in the SiGe NMs after release and transfer to new handling substrates (thermally oxidized Si [sample 1] or clean Si with chemical oxide [sample 2]), we use these new substrates for subsequent growths to demonstrate the viability of the SiGe NMs as realistic high-quality substrates for additional epitaxy. We grew ~35 nm of Si on the smooth side (Figure 3C) of the $Si_{0.68}Ge_{0.32}$ NM (sample 1) with MBE. An example of the Raman spectrum from this heterostructure is shown in Figure 4C. The frequency shift of the strained-Si peak

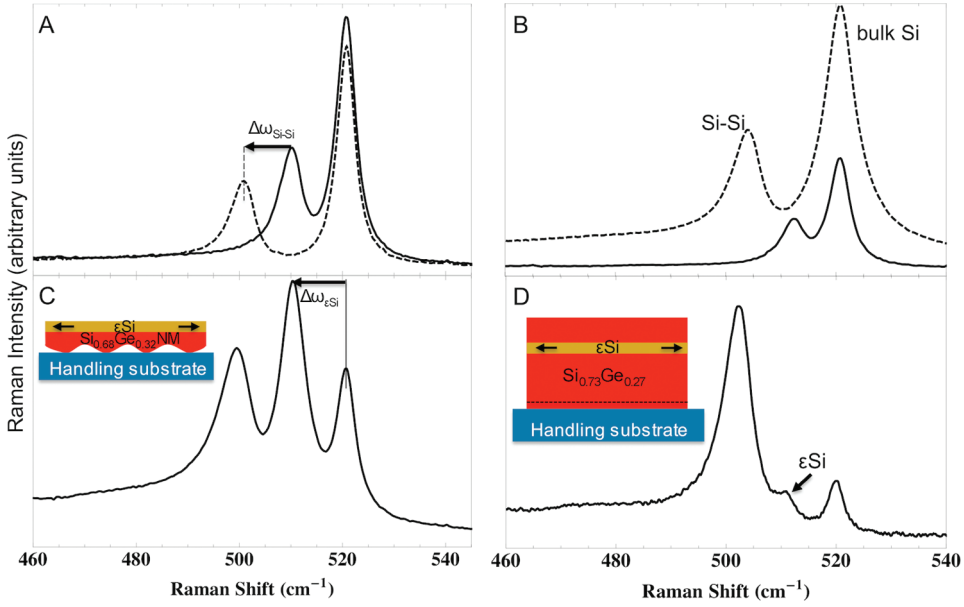

Figure 4. Raman spectra for SiGe NMs with two differing compositions and subsequent growths. (A) $Si_{0.68}Ge_{0.32}$ NM before (—) and after (– – –) release, and (B) $Si_{0.73}Ge_{0.27}$ NM before (—) and after (– – –) release. The shifts in the Si–Si peak ($\Delta\omega_{Si-Si}$) indicate full elastic relaxation of the strain. (C) Raman spectrum after ~35 nm strained-Si (εSi) overgrowth on the $Si_{0.68}Ge_{0.32}$ NM. (D) Spectrum after ~2 μm SiGe/10 nm εSi/20 nm SiGe overgrowth on the $Si_{0.73}Ge_{0.27}$ NM. The Si–Si peaks in (C) and (D) are consistent with the Si–Si peak positions after release of the SiGe NM [dashed lines in (A) and (B)]: the strain state of the SiGe NM does not change significantly after epitaxial overgrowth. The shift in the εSi peak to lower wavenumbers means the Si is tensilely strained. $\Delta\omega_{\varepsilon Si}$ is the Raman shift in the Si line due to the tensile lattice mismatch between the Si and the relaxed SiGe substrate. Raman spectra in (A), (B), and (C) are taken with a 532 nm laser, and the spectrum in (D) is taken with a 633 nm laser to penetrate the thick alloy layer. Intensities are plotted on a log scale. The intensity of each individual peak is proportional to the fraction of the total signal originating from that layer [*e.g.*, the εSi peak intensity is low in (D) because the εSi layer is very thin in proportion to the sampling depth (~3 μm for 633 nm laser)].

relative to the bulk-Si peak ($\Delta\omega_{\varepsilon Si}$) is in excellent agreement with the frequency shift of the Si–Si peak in the alloy layer from the as-grown compressive state of SiGe to the released and overgrown state of the SiGe NM (filled squares and open circles in Figure 5 lie on top of each other). This agreement is expected, as the frequency strain shift coefficients, *b*, agree within experimental uncertainty for the Si–Si mode of SiGe [b_{Si-Si} = 730 ± 70 cm^{-1})[34] and for strained Si [$b_{\varepsilon Si}$ = 723 ± 15 cm^{-1}].[35] The agreement in strain states means that we have grown coherently strained Si on a fully elastically relaxed Si NM substrate.

On the $Si_{0.73}Ge_{0.27}$ NM (sample 2), we grew, using CVD, a thick (~2 μm) lattice matched alloy buffer layer (matched to within 1 atomic % Ge composition; see Materials and Methods for details), followed by 10 nm of strained Si, and capped by ~20 nm of $Si_{0.73}Ge_{0.27}$. A Raman spectrum from this heterostructure is shown in Figure 4D. Again, for the same reasons as described above, the shift of the strained Si layer peak relative to the peak for unstrained Si (shaded squares in Figure 5) agrees with the peak shift in the Si–Si mode of the SiGe alloy from the compressively strained as-grown state to the elastically relaxed released state (open circles in Figure 5).

We grew the thick lattice-matched SiGe alloy on sample 2 to demonstrate that it is, in fact, possible to use the SiGe membrane as a growth substrate for making a macroscopic defect-free SiGe crystal. If the Ge composition of the epitaxial layer is perfectly matched, we could, in principle, continue growth to any thickness, as there is no strain in the system. Small deviations from the SiGe NM Ge composition will produce small amounts of strain in the epitaxial layer; however, even several micrometers of material are below the kinetic critical thickness for a film with a very small mismatch strain.[21] A 2 μm film is sufficient to allow us to use XRD to investigate the strain state of the alloy and check for strain variations from unexpected extended defects in the film. Figure 6 shows an XRD reciprocal-space map (RSM) around the (224) reflection of the SiGe grown on the elastically relaxed SiGe NM (recall there is also a 10 nm strained Si layer buried in the SiGe; see also below). We were able to separate the SiGe adventitiously grown on the surrounding bulk Si (support wafer) from that grown on the SiGe NM because the NM was bonded at a large in-plane twist angle with respect to the bulk Si support substrate. A twist angle means that any off-axis reflections from the bulk are at Bragg conditions different from those of the NM. The sharp SiGe peak in the RSM in Figure 6 indicates that there is very little strain variation over the sample area (~1 mm × 1 mm) or through the thickness of the alloy layer. There is no measurable mosaic broadening in this sample. For comparison, even the best material from strain-graded layer growth

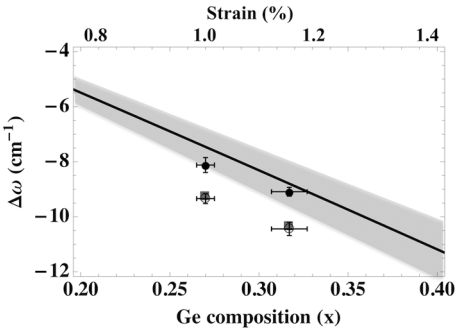

Figure 5. Frequency shift of the Si−Si mode in the SiGe NM from the strained state as-grown on Si (001) to the released state. The line is an empirical model for the frequency shift for the Si−Si mode for a $Si_{1-x}Ge_x$ alloy grown pseudomorphically on a Si(001) substrate as a function of Ge concentration, *x* (mismatch strain is a function of *x*). The shaded region encompasses the uncertainty in the model.[34] The filled circles (●) show the experimental frequency shift for the Si−Si mode in the SiGe NMs from the as-grown state to the released state ($\Delta\omega_{Si-Si}$). The open circles (○) are the same Si−Si mode frequency shifts of the SiGe(001) layer after lattice-matched alloy overgrowth or strained Si overgrowth on similar SiGe(001) NMs. The filled squares (■) are the frequency shifts of the εSi layer with respect to the bulk Si ($\Delta\omega_{\varepsilon Si}$). All frequency shifts are negative, indicating a biaxial expansion of the film with respect to the reference: the Si−Si as-grown peak position for SiGe NMs and bulk Si for the strained Si layers.

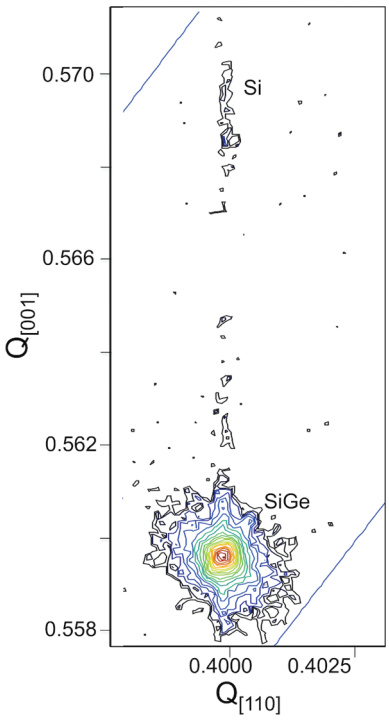

Figure 6. Reciprocal-space map (RSM) near the (224) reflection of ~20 nm $Si_{0.73}Ge_{0.27}$/10 nm Si/~2 μm $Si_{0.73}Ge_{0.27}$/$Si_{0.73}Ge_{0.27}$ NM. The most intense peak is from the SiGe NM and lattice-matched SiGe grown on top. The less intense peak is from the thin (~10 nm) strained Si layer of the heterostructure. There is no measurable mosaic broadening in any of the layers.

(one of the methods to make SiGe discussed earlier) shows mosaic broadening of at least 0.1° in all layers grown on top of the graded SiGe substrate.[36]

Our thin (~10 nm) strained Si layer grown on the thick lattice matched SiGe on a SiGe NM also does not show signs of strain variation over the sample area (~1 mm × 1 mm). This result is indicated by the sharp strained-Si layer peak located above the SiGe peak in the RSM of Figure 6. There is peak broadening in the out-of-plane (vertical) direction as a result of the thinness of the layer, but no significant broadening in the in-plane direction is detected. The agreement in horizontal peak position in reciprocal space (*i.e.*, lies on a vertical line with SiGe) confirms that the Si layer is fully strained to the same in-plane lattice constant as the relaxed SiGe NM "substrate".

The above heterostructure demonstrates that we can create a thin tensile-strained Si layer surrounded by relaxed SiGe, which is necessary for formation of a two-dimensional electron gas (2DEG), with the strained-Si layer being the quantum well for electrons.[2] To date, the best 2DEGs in the Si/SiGe system have been fabricated on graded buffer layers[37] that have the problems enumerated above. While the low-temperature charge carrier mobility in strained-Si 2DEGs is not in theory limited by the strain inhomogeneities, threading dislocation density, or interface roughness typical of these structures,[18] locally (length scales tens to hundreds of nanometers), the electrostatic potential is altered near these defects. Changes in the local disorder potential due to strain variations, as well as threading dislocations and interface roughness, are important for the fabrication of quantum dot devices (lateral areas ~300 nm) on 2DEGs in strained Si.[38] For example, local strain variations change the energy "depth" of the Si quantum well,[2] threading dislocations create trap states for charge carriers,[19] and interface roughness can alter the valley splitting in the conduction band due to quantum confinement.[39,40] In other words, if many quantum dot devices are fabricated on the same sample (working toward quantum computing),[9,25] any variations in these factors will cause each device to operate differently. In individual quantum devices, local strain variation may prove to be a limiting mechanism for spin decoherence times.[9] Thus, substrate inhomogeneity imposes yet another challenge to the ultimate goal of quantum computing. If our SiGe NMs are used to grow the heterostructures needed for strained Si 2DEG fabrication, we anticipate a large reduction in lateral variations of the disorder potential because we have removed surface roughness, strain variations, and threading dislocations from the material.

The exceptional crystalline quality of our SiGe NMs is demonstrated with the growth of ~35 nm of strained Si on sample 1 ($Si_{0.68}Ge_{0.32}$ NM); this thickness is above the equilibrium critical thickness for dislocation formation in ~1.2% tensilely strained Si.[41] While is has been

shown many times that the experimentally observed critical thickness of SiGe on high-quality, bulk Si(001) is larger than that of the equilibrium condition (due to kinetic limitations),[21] the experimentally observed critical thickness for dislocation formation of strained Si grown on (plastically) relaxed SiGe grown by step grading or condensation is much closer to the thermodynamic limit.[42] The observed differences are most likely related to the crystalline quality of the starting substrates. A Si wafer has very few defects to help nucleate dislocations at the Si/SiGe growth interface. In contrast, relaxed SiGe substrates have many threading dislocations that reach the surface and therefore lower the energy barrier to misfit dislocation formation at the SiGe/strained Si interface. For our SiGe NMs, there are no threading arms to help nucleate misfit dislocations; there is thus a higher potential barrier to dislocation formation, much like the case for SiGe grown on pure bulk Si. The increase in "kinetic" critical thickness that we observe for strained Si grown on SiGe NMs is also an advantage in the formation of strained-Si 2DEG devices because now we have a larger range of thicknesses within which we can tune the thickness of the Si well, while keeping the Si fully strained. This is an important consideration in the design of strained-Si 2DEGs, as it has been shown that any misfit dislocations formed at the strained-Si/SiGe interface (in contrast to ones in the bulk of SiGe as mentioned above) can significantly reduce charge carrier mobility.[43]

CONCLUSIONS

We have demonstrated the fabrication and use of elastically relaxed, single-crystalline $Si_{1-x}Ge_x$ NMs. The SiGe NMs are epitaxially grown below the critical thickness for defect-mediated relaxation on silicon-on-insulator substrates and subsequently released through two selective etching processes. We confirm with multiple characterization methods that the SiGe layers are fully strained to the Si lattice constant before release of the NM and fully relaxed to the SiGe lattice constant after release. Once transferred and bonded to new handling substrates, the SiGe NMs can be used as templates for growth of new material. We have demonstrated the growth of thick lattice matched SiGe alloy and Si coherently strained to the underlying SiGe NM. These experiments show that the SiGe NMs are suitable for growth of defect-free materials for use in high-performance applications.

The fabrication of defect-free single-crystalline SiGe also facilitates the integration of other semiconducting materials into existing Si technology. With a tunable-lattice-constant substrate, III−V and II−VI alloys can be grown with a matching lattice constant to incorporate direct band gap materials onto Si without the problems associated with lattice mismatched epitaxial growth. Control over the lattice constant of direct band gap materials allows tunability of the band gap to fabricate various optical devices, each operating at a different wavelength.

The procedure we have described is quite naturally extendable to other materials systems. The only requirements are that a film can be pseudomorphically grown on a single-crystal sheet, and that an etching method exists that can preferentially remove this sheet to allow the grown film to relax elastically. It can then be used as the new substrate. In particular, a whole menagerie of compound-semiconductor materials, as well as various complex ferroic and superconducting oxides, fits into this category. We can therefore expect that many new or better materials will become possible based on nanomembrane strain engineering.

MATERIALS AND METHODS

SiGe NM Fabrication. SiGe NM fabrication starts with molecular beam epitaxy (MBE) growth of thin SiGe alloy films on SOI(001) substrates with a ~25 nm top Si template layer and 150 nm buried oxide (BOX) layer. We resistively heat the substrate to 470 °C during pseudomorphic growth of the alloy and used a growth rate ~3 nm/min. The alloy layer thickness is kept below the kinetic critical thickness for dislocation-mediated relaxation of SiGe grown on Si.[21] Because the kinetic critical thickness is higher at lower temperatures, we use a low growth temperature; still lower temperatures can be used and will allow us to expand the range of compositions from what is described here. Immediately following the SiGe film growth, a Si capping layer of similar thickness as the SOI template layer is grown on top. At this point, we have a trilayer heterostructure consisting of Si/SiGe/Si, where the SiGe in-plane lattice parameter is strained to that of the Si lattice constant (Figure 1A).

Although the strain-driven roughening in our initial SiGe film may produce small variations in the Ge concentration[46] and hence strain laterally at the growth front of the SiGe film grown on SOI (strain variations of less than 0.2%), the initial growth interface (SiGe/SOI) and the smooth wetting layer will be at the nominal composition. In fact, the average Ge composition of the surface variations will be the same as the composition of the initial planar growth: larger Ge concentration at the peaks and smaller Ge concentration in the valleys. Lateral-strain variation effects in the rough surface of those samples that are grown to roughness are small and do not affect any conclusions.

The SiGe NM is elastically relaxed and released from the SOI substrate in two steps. [1] We etch away the BOX layer in 49% hydrofluoric acid (HF). To increase the etch rate we use an array of access holes to the oxide, but that is not essential. When fully released, the trilayer heterostructure comes to an equilibrium lattice constant and rests on the bulk (Si) handling substrate: elastic strain sharing occurs between the three layers, causing the trilayer to expand laterally.[22] The NMs are typically ~1 mm × 1 mm square. At this intermediate stage, the SiGe layer is still slightly compressively strained (Figure 1B). [2] We put the trilayer Si/SiGe/Si structure (resting on the bulk handling substrate) into dilute potassium hydroxide (KOH) solution: 45% KOH, dionized (DI) water, and isopropyl alcohol (IPA), with volume mixing ratio KOH/DI water/IPA = ~1:4:4.[24] Because the Si/SiGe/Si structure is only loosely bound (van der Waals force) to the underlying Si handling substrate, it immediately separates from the substrate and is suspended in the KOH solution.

For a sufficiently high Ge content in the SiGe film ($x > 20\%$), the outer Si layers in the trilayer membrane will etch much faster in the KOH solution than the SiGe (etch selectivity for $Si:Si_{0.8}Ge_{0.2}$ in KOH ~200:1),[44] leaving the SiGe NM fully elastically relaxed and suspended in solution (Figure 1C). The SiGe NM is rinsed in DI water, transferred, and bonded to a new Si handling substrate for subsequent growths (Figure 1D). Sample 1 ($Si_{0.68}Ge_{0.32}$ NM) was transferred to a thermally oxidized bulk Si wafer (~500 nm SiO_2 on top), and sample 2 ($Si_{0.73}Ge_{0.27}$ NM) was transferred to a Piranha cleaned (see below for details) Si wafer with only a chemical oxide on top. Bonding is encouraged by slowly annealing the sample to 500 °C on a hot plate.

For high Ge concentrations ($x > 30\%$), we flip the SiGe NM during the transfer process such that we bond the "rough" side of the NM to the new handling substrate, exposing the "smooth" side of the NM (initially the SiGe/SOI interface) for subsequent growths. We can determine the top and bottom surfaces of the SiNM optically by patterning an array of asymmetric etchant access holes.[24] An example of the asymmetric etchant access hole pattern is shown in the optical micrograph in Figure 3C.

Epitaxial Overgrowth on SiGe NMs. Once the SiGe NMs have been transferred and properly bonded to new handling substrates, the samples must be chemically cleaned *ex situ* before epitaxial growth. Our standard chemical cleaning procedure before growth on Si is as follows: [1] 20 s in 10% HF, [2] 10 min in Piranha clean (~80 °C $H_2SO_4 + H_2O_2$ solution), [3] 15 min in standard clean 1 [SC1] (~80 °C $H_2O + NH_4OH + H_2O_2$ solution), and [4] 20 s in 10% HF (with a 5 min DI water rinse between each step) before putting the sample directly into the high-vacuum growth chamber. However, the thin (~50 nm), high-Ge-concentration ($x > 20\%$) SiGe NMs are completely etched away in the 15 min SC1 solution. Therefore, we modify the chemical clean for the SiGe NM samples by using two cycles of 20 s in 10% HF + 10 min in Piranha solution. This cleaning procedure only etches away a few nanometers of the SiGe NM. We end the cleaning process with a 20 s 10% HF dip to remove any oxide that formed during the cleaning process and H-terminate the surface before inserting the sample into the high-vacuum growth chamber. We can use either MBE or chemical vapor deposition (CVD) for subsequent growths on the SiGe NMs. The layer on sample 1 (~35 nm Si on a $Si_{0.68}Ge_{0.32}$ NM) was grown with MBE at a growth rate ~3 nm/min, and that on sample 2 (~20 nm $Si_{0.73}Ge_{0.27}$/10 nm Si/~2 μm $Si_{0.73}Ge_{0.27}$ on a $Si_{0.73}Ge_{0.27}$ NM) was grown with CVD with an alloy growth rate of ~12 nm/min and a Si growth rate of ~4 nm/min. We performed several calibration growths before growing a thick, lattice-matched alloy layer on sample 2 to ensure that we matched the Ge composition to within 1% of the SiGe NM composition. The SiGe calibration samples were grown on Si substrates (to thicknesses less than the critical thickness) under the same growth conditions. The Ge composition was extracted from XRD measurements similar to those taken on the as-grown SiGe films for NM fabrication (see next section).

Characterization Methods. *X-ray Diffraction (XRD).* The initial strain state of the trilayer heterostructure (Si/SiGe/Si) was characterized with high-resolution XRD (Phillips Panalytical X'Pert PRO). The $\theta/2\theta$ lines scans around the (004) reflection were fit to simulation to extract the Ge composition of the SiGe layer and each of the layer thicknesses before release from the initial growth substrate. RSMs around off-axis reflections (224) give us insight into strain variation in the in-plane lattice constant before release of the SiGe NM (Figure 2B,C) and after overgrowth (Figure 6).

Atomic Force Microscopy (AFM). Intermittent-contact mode AFM (Digital Instruments Nanoscope IIIa) was used to characterize the surface morphology of the top and bottom surfaces of the SiGe NMs to check for 3D nanocrystal formation.

Raman Spectroscopy. We use laser wavelengths of ~532 nm or ~633 nm (LabRAM Aramis Horiba Jobin Yvon Confocal Raman Microscope) to ensure that the incident radiation penetrates the entire thickness of the SiGe NM and any epitaxial layer grown on top. It is then possible to use the bulk-Si peak (normalized to 520.0 cm^{-1}) from the underlying substrate as a reference peak in all Raman spectra. The peak positions are determined by fitting the bulk-Si peak with a pseudo-Voigt symmetric functional form, and the Si−Si peak with an asymmetric functional form.[45] The frequency shifts are an average of four or more measurements taken over a ~1 mm × 1 mm area on each sample, and the uncertainty is the standard deviation of these measurements.

Acknowledgment. This research is funded by DOE, Grant No. DE-FG02-03ER46028. Facilities support by NSF, MRSEC program, is acknowledged. D.M.P. acknowledges support from the NSF Graduate Research Fellowship Program.

REFERENCES AND NOTES

1. Paul, D. J. Si/SiGe Heterostructures: From Material and Physics to Devices and Circuits. *Semicond. Sci. Technol.* **2004**, *19*, R75–R108.
2. Schäffler, F. High-Mobility Si and Ge Structures. *Semicond. Sci. Technol.* **1997**, *12*, 1515–1549.
3. Lee, M. L.; Leitz, C. W.; Cheng, Z.; Pitera, A. J.; Langdo, T; Currie, M. T.; Taraschi, G.; Fitzgerald, E. A.; Antoniadis, D. A. Strained Ge Channel p-Type Metal-Oxide-Semiconductor Field-Effect Transistors Grown on $Si_{1-x}Ge_x$/Si Virtual Substrates. *Appl. Phys. Lett.* **2001**, *79*, 3344–3346.
4. Xia, G.; Hoyt, J. L.; Canonico, M. Si−Ge Interdiffusion in Strained Si/Strained SiGe Heterostructures and Implications for Enhanced Mobility Metal-Oxide-Semiconductor Field-Effect Transistors. *J. Appl. Phys.* **2007**, *101*, 044901.
5. Chu, M.; Sun, Y.; Aghoram, U.; Thompson, S. E. Strain: A Solution for Higher Carrier Mobility in Nanoscale MOSFETs. *Annu. Rev. Mater. Res.* **2009**, *39*, 203–229.
6. Sun, Y.; Thompson, S. E.; Nishida, T. Physics of Strain Effects in Semiconductors and Metal-Oxide-Semiconductor Field-Effect Transistors. *J. Appl. Phys.* **2007**, *101*, 104503.
7. Jacobsen, R. S.; Andersen, K. N.; Borel, P. I.; Fage-Pedersen, J.; Frandsen, L. H.; Hansen, O.; Kristensen, M.; Lavrinenko, A. V.; Moulin, G.; Ou, H.; *et al.* Strained Silicon as a New Electro-optic Material. *Nature* **2006**, *441*, 199–202.
8. Xie, Y. H.; Fitzgerald, E. A.; Monroe, D.; Silverman, P. J.; Watson, G. P. Fabrication of High Mobility Two-Dimensional Electron and Hole Gases in GeSi/Si. *J. Appl. Phys.* **1993**, *73*, 8364–8370.
9. Simmons, C. B.; Prance, J. R.; Van Bael, B. J.; Koh, T. S.; Shi, Z.; Savage, D. E.; Lagally, M. G.; Joynt, R.; Friesen, M.; Coppersmith, S. N.; *et al.* Tunable Spin Loading and T_1 of a Silicon Spin Qubit Measured by Single-Shot Readout. *Phys. Rev. Lett.* **2011**, *106*, 156804.
10. Borselli, M. G.; Ross, R. S.; Kiselev, A. A.; Croke., E. T.; Holabird, K. S.; Deelman, P. W.; Warren, L. D.; Alvarado-Rodiguez, I.; Milosavljevic, I.; Ku, F. C.; *et al.* Measurement of Valley Splitting in High-Symmetry Si/SiGe Quantum Dots. *Appl. Phys. Lett.* **2011**, *98*, 123118.
11. Oh, H. J.; Choi, K. J.; Loh, W. J.; Htoo, T.; Chua, W. J.; Cho, B. J. Intergration of GaAs Epitaxial Layer to Si-Based Substrate Using Ge Condensation and Low-Temperature Migration Enhanced Epitaxial Techniques. *J. Appl. Phys.* **2007**, *102*, 054306.
12. Bolkhovityanov, Y. B.; Pchelyakov, O. P. GaAs Epitaxy on Si Substrates: Modern Status of Research and Engineering. *Phys.-Usp.* **2008**, *51*, 437–456.
13. Hartmann, J. M.; Gallas, B.; Zhang, J.; Harris, J. J.; Joyce, B. A. Strain-Balanced Si/SiGe Short Period Superlattices: Disruption of the Surface Crosshatch. *J. Appl. Phys.* **1999**, *86*, 845–849.
14. Borak, A.; Tsujino, S.; Falub, C.; Scheinert, M.; Diehl, L.; Müller, E.; Sigg, H.; Grützmacher, D.; Gennser, U.; Sagnes, I.; *et al.* Recent Results on the Road to a SiGe Quantum Cascade Laser. *Mater. Res. Soc. Symp. Proc.* **2005**, *832*, F4.2.1.
15. Schilz, J.; Romanenko, V. N. Bulk Growth of Silicon−Germanium from Solid Solutions. *J. Mater. Sci.: Mater. Electron.* **1995**, *6*, 265–279.
16. Tezuka, T.; Sugiyama, N.; Takagi, S. Fabrication of Strained Si on Ultrathin SiGe-on-Insulator Virtual Substrate with a High-Ge Fraction. *Appl. Phys. Lett.* **2001**, *79*, 1798–1800.

17. Terzieva, V.; Souriau, L.; Clemente, F.; Benedetti, A.; Caymax, M.; Meuris, M. The Challenges of Ge-Condensation Technique. *ECS Trans.* **2006**, *3*, 1023–1031.
18. Monroe, D.; Xie, Y. H.; Fitzgerald, E. A.; Silverman, P. J.; Watson, G. P. Comparison of Mobility-Limiting Mechanisms in High-Moblity $Si_{1-x}Ge_x$ Heterostructures. *J. Vac. Sci. Technol., B* **1993**, *11*, 1731–1737.
19. Holt, D. B.; Yacobi, B. G. *Extended Defects in Semiconductors: Electronic Properties, Device Effects and Structures*; Cambridge University Press: Cambridge, MA, 2007.
20. Thalakulam, M.; Simmons, C. B.; Rosemeyer, B. M.; Savage, D. E.; Lagally, M. G.; Friesen, M.; Coppersmith, S. N.; Eriksson, M. A. Fast Tunnel Rates in Si/SiGe One-Electron Single and Double Quantum Dots. *Appl. Phys. Lett.* **2010**, *96*, 183104.
21. Houghton, D. C. Strain Relaxation Kinetics in $Si_{1-x}Ge_x$/Si Heterostructures. *J. Appl. Phys.* **1991**, *70*, 2136–2151.
22. Roberts, M. M.; Klein, L. J.; Savage, D. E.; Slinker, K. A.; Friesen, M.; Celler, G.; Eriksson, M. A.; Lagally, M. G. Elastically Relaxed Free-Standing Strained-Silicon Nanomembranes. *Nat. Mater.* **2006**, *5*, 388–393.
23. Mo, Y.-W.; Savage, D. E.; Swartzentruber, B. S.; Lagally, M. G. Kinetic Pathway in Stranski-Krastanov Growth of Ge on Si(001). *Phys. Rev. Lett.* **1990**, *65*, 1020–1023.
24. Tanto, B. Dislocation-Free Strain-Engineered Si and SiGe Nanomembranes. PhD Dissertation; University of Wisconsin—Madison, 2009.
25. Shaji, N.; Simmons, C. B.; Thalakulam, M.; Klein, L. J.; Qin, H.; Luo, H.; Savage, D. E.; Lagally, M. G.; Rimberg, A. J.; Joynt, R.; *et al.* Spin Blockcade and Lifetime-Enhanced Transport in a Free-Electron Si/SiGe Double Quantum Dot. *Nat. Phys.* **2008**, *4*, 540–544.
26. Huang, M.; Rugheimer, P.; Lagally, M. G.; Liu, F. Bending of Nanoscale Ultrathin Substrates by Growth of Strained Thin Films and Islands. *Phys. Rev. B* **2005**, *72*, 085450.
27. Eaglesham, D. J.; Hull, R. Island Formation in Ge/Si Epitaxy. *Mater. Sci. Eng., B* **1995**, *30*, 197–200.
28. Steinfort, A. J.; Scholte, P. M. L. O.; Ettema, A.; Tuinstra, F. Strain in Nanoscale Germanium Hut Clusters on Si(001) Studied by X-ray Diffraction. *Phys. Rev. Lett.* **1996**, *77*, 2009–2012.
29. Floro, J. A.; Chason, E.; Freund, L. B.; Twesten, R. D.; Hwang, R. Q.; Lucadamo, G. A. Evolution of Coherent Islands in $Si_{1-x}Ge_x$/Si(001). *Phys. Rev. B* **1999**, *59*, 1990–1998.
30. Tersoff, J.; LeGoues, F. K. Competing Relaxation Mechanisms in Strained Layers. *Phys. Rev. Lett.* **1994**, *72*, 3570–3573.
31. Eaglesham, D. J.; Cerullo, M. Dislocation-Free Stranski-Krastanov Growth of Ge on Si(100). *Phys. Rev. Lett.* **1990**, *64*, 1943–1946.
32. Bean, J. C.; Feldman, L. C.; Fiory, A. T.; Nakahara, S.; Robinson, I. K. Ge_xSi_{1-x}/Si Strained-Layer Superlattice Grown by Molecular Beam Epitaxy. *J. Vac. Sci. Technol., A* **1984**, *2*, 436–440.
33. De Wolf, I. Micro-Raman Spectroscopy to Study Local Mechanical Stress in Silicon Integrated Circuits. *Semicond. Sci. Technol.* **1996**, *11*, 139–154.
34. Pezzoli, F.; Bonera, E.; Grilli, E.; Guzzi, M.; Sanguinetti, S.; Chrastina, D.; Isella, G.; von Känel, H.; Wintersberger, E.; Stangl, J.; *et al.* Phonon Strain Shift Coefficients in $Si_{1-x}Ge_x$ Alloys. *J. Appl. Phys.* **2008**, *103*, 093521.
35. Nakashima, S.; Mitani, T.; Ninomiya, M.; Matsumoto, K. Raman Investigation of Strain in Si/SiGe Heterostructures: Precise Determination of the Strain-Shift Coefficient of Si Bands. *J. Appl. Phys.* **2006**, *99*, 053512.
36. Mooney, P. M.; Chu, J. O. SiGe Technology: Heteroepitaxy and High-Speed Microelectronics. *Annu. Rev. Mater. Sci.* **2000**, *30*, 335–362.
37. Lu, T. M.; Tsui, D. C.; Lee, C.-H.; Liu, C. W. Observation of Two-Dimensional Electron Gas in a Si Quantum Well with Mobility of 1.6×10^6 cm^2/V s. *Appl. Phys. Lett.* **2009**, *94*, 182102.
38. Goswami, S.; Slinker, K. A.; Friesen, M.; McGuire, L. M.; Truitt, J. L.; Tahan, C.; Klein, L. J.; Chu, J. O.; Mooney, P. M.; Van der Weide, D. W.; *et al.* Controllable Valley Splitting in Silicon Quantum Devices. *Nat. Phys.* **2007**, *3*, 41–45.
39. Kharche, N.; Prada, M.; Boykin, T. B.; Klimeck, G. Valley Splitting in Strained Silicon Quantum Wells Modeled with 2° Miscuts, Step Disorder, and Alloy Disorder. *Appl. Phys. Lett.* **2007**, *90*, 092109.
40. Chen, F.; Ramayya, E. B.; Euaruksakul, C.; Himpsel, F. J.; Celler, G. K.; Ding, B.; Knezevic, I.; Lagally, M. G. Quantum Confinement, Surface Roughness, and the Conduction Band Structure of Ultrathin Silicon Membranes. *ACS Nano* **2010**, *4*, 2466–2474.
41. Matthews, J. W.; Blakeslee, A. E. Defects in Epitaxial Multilayers: I. Misfit Dislocations. *J. Cryst. Growth* **1974**, *27*, 118–125.
42. Samavedam, S. B.; Taylor, W. J.; Grant, J. M.; Smith, J. A.; Tobin, P. J.; Dip, A.; Phillips, A. M.; Liu, R. Relaxation of Strained Si Layers Grown on SiGe Buffers. *J. Vac. Sci. Technol., B* **1999**, *17*, 1424–1429.
43. Ismail, K.; LeGoues, F. K.; Saenger, K. L.; Arafa, M.; Chu, J. O.; Mooney, P. M.; Meyerson, B. S. Identification of a Mobility-Limiting Scattering Mechanism in Modulation-Doped Si/SiGe Heterostructures. *Phys. Rev. Lett.* **1994**, *73*, 3447–3450.
44. Borenstein, J. T.; Gerrish, N. D.; White, R.; Currie, M. T.; Fitzgerald, E. A. Silicon Germanium Epitaxy: A New Material for MEMS. *Mater. Res. Soc. Symp.* **2001**, *657*, EE7.4.1.
45. Perova, T. S.; Wasyluk, J.; Lyutovich, K.; Kasper, E.; Oehme, M.; Rode, K.; Waldron, A. Composition and Strain in Thin $Si_{1-x}Ge_x$ Virtual Substrate Measured by Micro-Raman Spectroscopy and X-ray Diffraction. *J. Appl. Phys.* **2011**, *109*, 033502.
46. Wu, C.-C.; Hull, R. Composition and Stress Fields in Undulated $Si_{0.7}Ge_{0.3}$/Si(100) Thin Films. *J. Appl. Phys.* **2006**, *100*, 083510.